Please cite the following article as:

Kam, S., Cepeda-Salgado, B., Lee, G., & Tsai, F. (2026). A novel surfactant-enhanced DNAPL remediation technology with horizontal wells. *InterPore Journal*. Advance online publication. https://doi.org/10.69631/241eb066

Received on: 14 Oct. 2025
Accepted on: 15 Feb. 2026
Published online (Accepted version): 18 Mar. 2026

A Novel Surfactant-Imbibition DNAPL Remediation Technology with Horizontal Extraction Wells

Betty Cepeda-Salgado[1], Gyu S. Lee[2], Frank Tsai[3] and Seung I. Kam[1*]

[1]Louisiana State University, Craft and Hawkins Department of Petroleum Engineering, Baton Rouge, USA
[2]Rural Research Institute in Korea Rural Research Corporation, Ansan/Naju, South Korea
[3]Louisiana State University, Department of Civil and Environmental Engineering, Baton Rouge, USA

***Corresponding Author: kam@lsu.edu, 225-578-5216**

Abstract

This study investigates the feasibility of in-situ surfactant-imbibition DNAPL (Dense Non-Aqueous Phase Liquids) remediation methods, where the surfactant solution is drawn into the contaminated site from the top vertical wells which is driven by active extraction of formation fluids from the bottom horizontal wells. The fundamental mechanism of this novel technology is analyzed by using a dimensionless group (F) associated with capillary forces, combined with sweep efficiency.

By (i) matching the pattern of DNAPL plume leakage and spreading and (ii) analyzing the remediation efficiency in various design and optimization scenarios, this two-dimensional simulation study shows that the new technology can achieve the cumulative oil recovery 36 - 37 % more than simple water imbibition methods for 10 m horizontal well spacing (and 52 - 53 % more if the spacing can be adjusted down to 3 - 5 m). This improvement over the conventional water imbibition (that recovers a negligible amount of DNAPLs) results from the fact that the system configuration and design successfully create a sufficient pressure gradient for the surfactant solution to lower the level of capillary trapping and thus mobilize oil blobs, also generating contact areas large enough laterally to sweep the contaminants.

This study is the first step into the use of active horizontal extraction wells for in-situ DNAPL remediation with surfactant imbibition, prior to the testing of injecting gas and surfactant mixtures.

Keywords: surfactant imbibition, horizontal extraction wells, DNAPL, in-situ remediation, modeling and simulation

1.Introduction

1.1. Background

Groundwater can be polluted by infiltration of contaminants through sediments and soils, direct flow from fractures, improperly built wells, amongst others (21, 34). Contaminants that may stem from diverse backgrounds, whether naturally occurring or anthropogenic, can be classified as non-organic and organic contaminants. Of particular interest in this study are the immiscible organic contaminants, commonly known as non-aqueous phase liquids (NAPLs), which are relatively insoluble and thus tend to be trapped by the capillary forces in subsurface (21). Benzene, toluene, ethylbenzene, and xylene are examples of light NAPLs (or LNAPLs), while tetrachloroethylene (PCE) and trichloroethylene (TCE) are examples of dense NAPLs (or DNAPLs) (18). Once leaked, DNAPLs tend to migrate downwards, often well into the saturated zone, until they encounter impermeable capillary barriers (for example, shale layers). Such a property makes it difficult to recover DNAPL contaminants in actual in-situ remediation treatments (17).

One of the popular in-situ methods is the injection of surfactant chemicals dissolved in water, sometimes referred to as surfactant enhanced aquifer remediation (SEAR), which was initially proposed based on surfactant flooding research for enhanced oil recovery (EOR) as described by Lake 19). Small-scale flow experiments show that an addition of surfactants can increase the effectiveness of water injection by a couple of orders of magnitude (12, 23) through interfacial tension reduction and solubilization (15). These aspects are also well supported by computer simulation studies (5, 11). Successful field trials can be found in the literature, for example, DNAPL recovery from shallow aquifer in the Thouin Sand Pit (20), DNAPL treatment from an aquifer near disposal trenches in the Hill Air Force Base (4), spill treatments in a Marine Corps Base in Camp LeJeune (16), two successful remediation cases (including TCE) from Alameda Point and Spartan Chemical Company Superfund Site (32), PCE removal from a control test cell at the Dover National Test Site (8), jet fuel treatment from a sandy aquifer in Jutland (30), and LNAPL recovery underneath the military fuel distribution facilities (6, 14). SEAR techniques can be improved in conjunction with surfactant-foam processes as foaming the injected gas phase is shown to be often more efficient in the field with higher sweep efficiency (14, 33), with less liquid involved (25, 26), and with diverting and blocking capabilities (7).

Some in-situ treatments may have additional challenges, dealing with more complicated situations such as hilly terrains, existing man-made structures (e.g., buildings, underground facilities, roads, and railroads), and natural environments (rivers, reservoirs, and severe subsurface heterogeneity). Using inclined and horizontal wells (whether injection, extraction, or both) can be a viable option in these cases, inspired by the EOR method using horizontal wells, so-called gas-assisted gravity drainage (or GAGD; 24). Some examples can be found in the literature, for instance, Sawyer and Lieuallen-Dulama (29) performing a productivity analysis comparing horizontal and vertical extraction well configurations for a simulated contaminated aquifer; Allouche et al. (1) reporting two field cases where horizontal wells were successful with remediation activities (an Airforce base in Arizona and a pumping station in California); Moran and Logonsky (22) applying ten horizontal wells

(instead of nearly 100 vertical wells) to remediate a TCE contaminated area below a dry cleaner in a shopping mall; NAVFAC technical report by Rosansky (27) conveying a field application of a combination of horizontal and vertical wells for remediation of DNAPLs in a naval facility in Maryland; Bortone et al. (2) investigating vertical and horizontal wells for a pump-and-treat operation through 3D modelling; and Feng et al. (13) examining the performance of a multi-branch horizontal remediation well technique in Jiangsu Province, China.

1.2. Objective of this study

This study investigates a spill site located in a hilly terrain within a military base in the Republic of Korea. Efforts have been made to identify the contaminants (both light and dense NAPLs) and the extent of the contaminant plumes, as shown in Figure 1 and Figure 2. The first major location is the flat ground area denoted by "(A)" (at lower elevation at the eastern side) with shallow subsurface contaminants. This is the area where an ex-situ remediation process is suitable for. The second major location is the area ranging from the hill top with storage tanks (at higher elevation at the western side) to the slope (denoted by "(D)") connecting to the ground (A). The area with a steep slope (D) is contaminated by a mixture of light and dense NAPLs, originating from the storage tanks (the hill top) as the leak source.

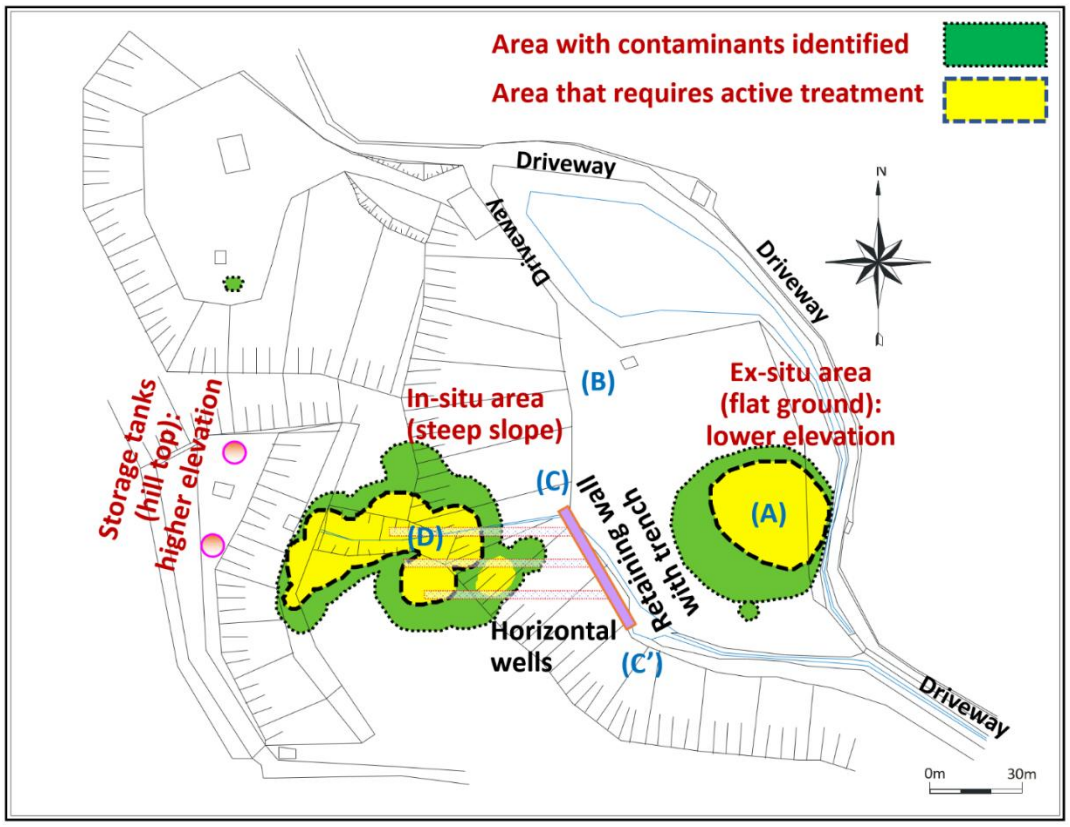

Figure 1 Topographic map of the military base with contaminated areas identified

Figure 2 Photos showing the military base (A, B, C, C' and D corresponding to those in the topographic map)

For the new technique examined in this study (i.e., vertical surfactant-imbibition wells and horizontal extraction wells), processing facilities for the treatment of extracted fluids and separation of surfactant solutions (to be recycled and re-imbibed) are located near the flat ground, shown by "(B)." Three horizontal wells, constructed slightly above the ground level into the retaining wall, are connected to the pumping units that direct extracted fluid mixtures to the processing facilities. A trench (parallel to the retaining wall and roughly perpendicular to the horizontal wells) is constructed, as shown by the line connecting "(C)" and "(C')," to collect and monitor the groundwater samples during the operations.

When the leaking contaminant mixtures seep down into the soil at the hill top, there is a natural separation of NAPLs vertically based on the density. In addition, the contaminants spread to the east (and slightly to the south as well) following the hydraulic pressure gradient. Tests from soil and underground water samples, together with resistivity logs, allow NAPL distribution to be mapped over the 5 m depth (96 through 101 meters above sea level) as shown in Figure 3. Naturally, the shallow plume (99 – 101 meter) consisting of LNAPLs is the candidate for the soil vapor extraction in-situ treatment, while the deep plume (96 – 99 meter and below) consisting of DNAPLs remains as a major challenge. (The red circles numbered in Figure 3 represent soil and water sampling wells in the field.)

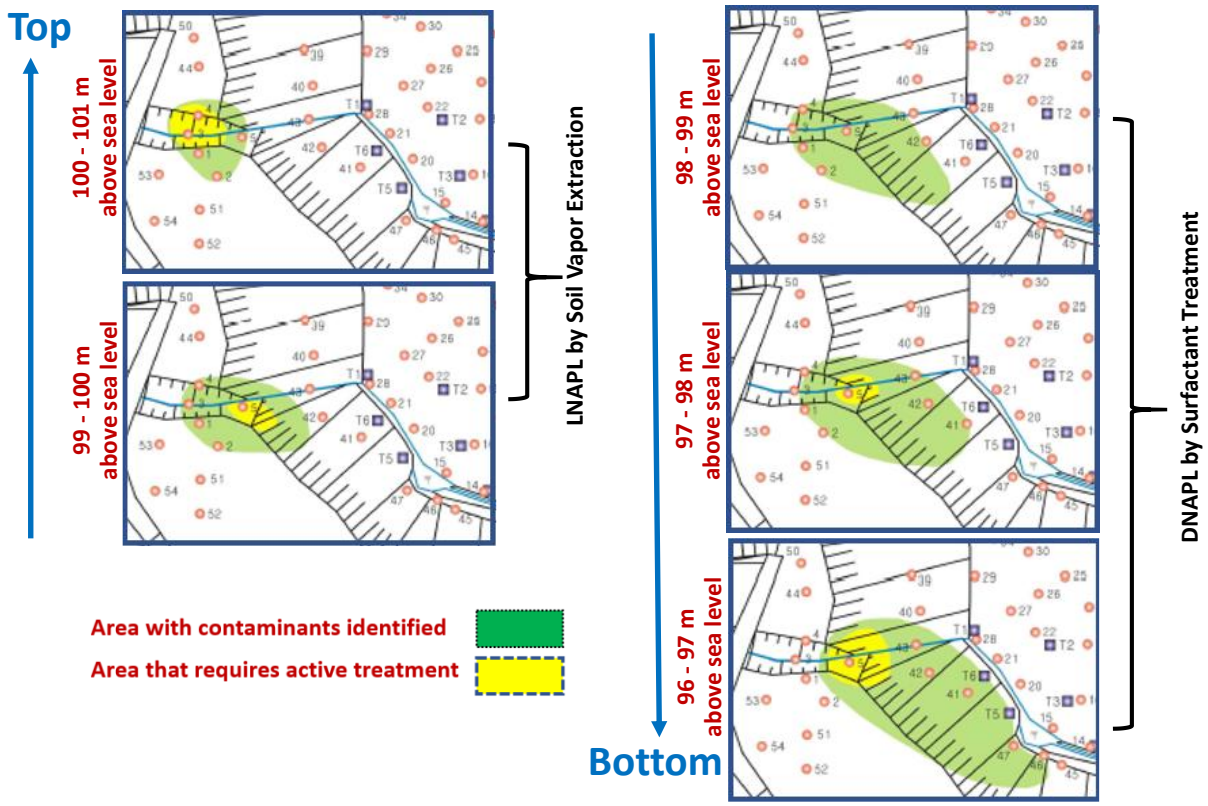

Figure 3 Distribution of total petroleum hydrocarbons (TPHs) from sampling and resistivity logs

Therefore, the objective of this study is to evaluate this new and innovative horizontal well technique for DNAPL remediation, and understand the primary mechanisms and parameters for the successful field applications. Figure 4 shows a simplified drawing of the field conditions with injection and extraction wells where the estimated oil spill volume is about 2,500 – 3,500 liters (i.e., 2.5 - 3.5 m^3). The two-dimensional simulation of this study is determined to deal with a small representative vertical segment (40 m width and 10 m depth with 0.1 m thickness; see more details in Table 1 below), containing one-hundredth of the spill volume (this is, about 30 liters (0.030 m^3)). (The actual in-situ remediation efficiency for the duration of 2 months is estimated to be around 30 - 40 % NAPL recovery. The majority of the recovery was achieved during the first week of the operations, followed by additional recovery during the next few weeks (i.e., all these in about first 30 days or first month), while there was no significant recovery observed in the second month (second 30 days of operations).)

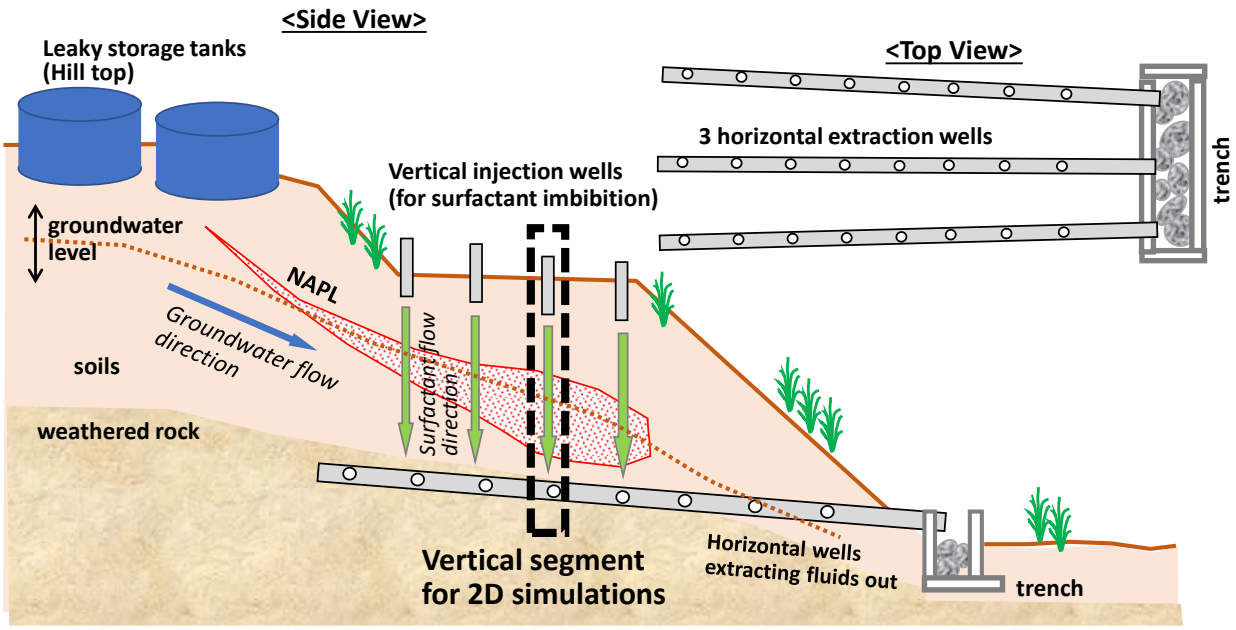

Figure 4 Drawing of leak and remediation events for the DNAPL contaminants

2. Materials and Methods

2.1. Fundamental mechanisms and associated equations

For multiphase and multi-component transient simulations, this study uses the Computer Modelling Group (CMG) reservoir simulation software (9) to solve for governing equations and related transport equations. Of particular use is the STARS subprogram for chemical process in which a phase may contain multiple components (for example, an aqueous phase with water and surfactant components in it, i.e., two-component and single-phase system). The governing partial differential equation solved by CMG for any component i within the system is shown below following mass balance (19):

$$\frac{\partial}{\partial t}\left(\phi\sum_{j=1}^{N_p}\rho_j S_j \omega_{ij} + (1-\phi)\rho_s \omega_{is}\right) + \nabla\cdot\left(\sum_{j}^{N_p}\rho_j \omega_{ij}\vec{u}_j - \phi S_j D_{ij}\nabla\omega_{ij}\right) = \phi\sum_{j=1}^{N_p} S_j r_{ij} + (1-\phi) r_{is}$$

for component i (1a)

where the subscripts i, j and s represent components, fluid phases and solid (as a phase), respectively. Also included are the porosity of the media (ϕ), density (ρ) and saturation (S) of the existing phases (with N_p the number of fluid phases present in the media), mass fraction of component i in phase j (ω_{ij}), velocity vector of phase j ($\vec{u}_j$), dispersion coefficient tensor ($\vec{D}_{ij}$), and chemical reactions within the fluid phases or at the solid surface (r_{ij} and r_{is}). The two terms on the left-hand side of the equation are related to accumulation and transport (convection and dispersion) for each component, while the term on the right-hand side represents reactions involving the fluid phases and solid. As the primary focus of this study

is to examine the recovery factor in an environment where the convection term is dominant, the adsorption to the solid surface (ω_{is}), dispersion ($\vec{D}_{ij}$) and reaction (r_{ij} and r_{is}) terms are turned off, making the material balance equation simplified as follows:

$$\frac{\partial}{\partial t}\left(\phi\sum_{j=1}^{N_p}\rho_j S_j \omega_{ij}\right)+\nabla\cdot\left(\sum_{j}^{N_p}\rho_j\omega_{ij}\vec{u}_j\right)=0$$

for component i (1b)

(CMG (9) also provides more detailed descriptions on the governing equation and related mathematical expressions and derivations (especially in Appendix F.2 and Appendix F.5).)

The main transport mechanism, in terms of convection, is expressed by Darcy's equation. For any phase j, the transport equation can be written as follows in a three-dimensional space:

$$\overrightarrow{u_j}=-\frac{Kk_{rj}}{\mu_j}(\nabla P_j-\rho_j g\nabla z) \qquad \text{for phase j} \qquad (2a)$$

which becomes as follows for a one-dimensional linear and horizontal flow, for example:

$$\frac{Q_j}{A}=u_j=\frac{Kk_{rj}}{\mu_j}\frac{\Delta P_j}{L} \qquad \text{for phase j} \qquad (2b)$$

where the flow rate is given by Q_j, cross-sectional area A, Darcy velocity u_j, fluid viscosity μ_j, absolute permeability K, relative permeability k_{rj}, g gravitational acceleration, z vertical coordinate, and pressure drop ΔP_j over the length of L (or, pressure gradient (∇P_j)). The two- and three-phase relative permeability functions (j = w for water or surfactant solution, o for oil, and g for gas phases) are defined as follows, by taking advantage of Corey's model (3) and Stone II model (31):

$$k_{rw}=k_{rw}^0\left(\frac{S_w-S_{wr}}{1-S_{wr}-S_{or}}\right)^m \qquad (3)$$

$$k_{rg}=k_{rg}^0\left(\frac{1-S_l-S_{gr}}{1-S_{wr}-S_{or}-S_{gr}}\right)^p \qquad (4)$$

$$k_{ro}=k_{ro}^0\left(\frac{S_o-S_{or}}{1-S_{wr}-S_{or}}\right)^n \qquad \text{(for two-phase flow)} \qquad \text{and} \qquad (5)$$

$$k_{ro}=k_{rw}^0\left(\left(\frac{k_{rw}^0}{k_{rw}^0+k_{rw}}\right)\left(\frac{k_{rog}}{k_{rw}^0+k_{rg}}\right)-k_{rw}-k_{rg}\right)$$

$$\text{with} \quad k_{rog}=k_{rog}^0\left(\frac{S_l-S_{or}-S_{wr}}{1-S_{wr}-S_{or}-S_{gr}}\right)^q \quad \text{(for three-phase flow)} \qquad (6)$$

where S_{wr}, S_{or}, and S_{gr} are the residual saturations; k_{rw}^0, k_{ro}^0, and k_{rg}^0 are the end-point relative permeability values; and m, n and p are the coefficients for water, oil and gas phases, with additional model parameters and variables (S_l, k_{rog}^0, k_{rog} and q). Note that the liquid

saturation S_l is no other than the sum of S_w and S_o. Therefore, the calculation deals with up to 3 phases and 4 (pseudo)components such as water (H_2O), surfactant (Tween80), oil (TCE), and gas (nitrogen).

Another important aspect to consider is the high capillary pressure (P_c) environments within the subsurface where these three immiscible phases interact with each other (19, 28). The capillary pressure (P_c) can be related to other properties such as interfacial tension (σ) between the phases, contact angle (θ), and average pore size (r_{pore}). Therefore, the capillary pressure between water and oil phases ($P_{c,ow}$), for example, can be described as follows, P_o and P_w being oil and water pressures:

$$P_{c,ow} = P_o - P_w = \frac{2\sigma_{wo}\cos\theta_{ow}}{r_{pore}} \quad . \tag{8}$$

Note that for oil blobs trapped within pores, the pressure drop must be sufficient enough (i.e., higher than the capillary pressure) to make the blobs mobilized (28). The presence of surfactant molecules helps this mobilization mechanism as they reduce the interfacial tension and thus capillary pressure. Similar descriptions are possible by using the concept of dimensionless capillary number (N_c), as CMG (9) conducts interpolations to obtain the relative permeability curves in the presence of surfactants. N_c is defined as follows (19):

$$N_c = \frac{u_w\,\mu_w\cos\theta_{ow}}{\sigma_{ow}} \tag{9}$$

Two sets of relative permeability curves are required for the CMG simulations (9) to handle 3 phase flow (in the absence of surfactant) in porous media: "k_{rw} (S_w) and k_{ro} (S_w)" and "k_{rw} (S_l) and k_{ro} (S_l)". In the presence of surfactant solution, CMG performs interpolations between the original sets of relative permeability curves (representing the case of σ_{ow} = 32 dyne/cm (no surfactant)) and the imaginary sets of relative permeability curves (reflecting near complete miscibility at a very low σ_{ow} by using linear lines). The natural logarithm of the dimensionless capillary number ($\ln(N_c)$), which is a function of σ_{ow}, is used as a tool for the interpolation calculations. (See CMG (9) for more detailed descriptions on how these three-phase relative permeability curve concepts are implemented in the simulation of chemical flooding, especially in Section D.6).)

Another pressure term that plays a role in is the hydrostatic pressure (P_h). With the vertical depth of h, fluid density (ρ), and gravitational acceleration (g), P_h can be given by the following equation:

$$P_h = \rho g h \quad . \tag{10}$$

The multiphase and multi-component transient simulations are performed using the Computer Modelling Group (CMG) STARS subprogram, which can handle thermal and chemical processes. The full formulation of all equations and background artifacts is provided in the CMG STARS manual (9).

2.2. Description of the system

The purpose of this research associated with the new in-situ remediation technology is to understand how the combined mechanisms (i.e., vertical surfactant-imbibition wells and horizontal extractions wells) would work together, by investigating a two-dimensional cross-section (See the vertical plane segment in Figure 4) that contains one vertical well (for surfactant imbibition) and three horizontal wells (for formation-fluid extraction), as shown in Figure 5. The system (which has the dimension of length L, height H, and width W) consists of N_x, N_z, and N_y number of grid blocks, respectively (note that x (horizontal) and z (vertical) directions are the major axes of interest). $N_y = 1$ (along the y direction), of course, in this 2D simulation approach, while N_x is any reasonably large "odd" number such that $[(N_x + 1)/2]^{th}$ grid blocks represent the middle vertical line of the grid system. Note that the injection well (that extends from the top of the soil to the vertical depth of H_{inj} with the radius of r_{inj}) and the middle extraction well (that is called EW#2 with the radius of r_{ext}) are positioned along the middle vertical line. Two other extraction wells such as EW#1 and EW#3 are located L_{sp} distance (i.e., spacing between the horizontal wells) away from EW#2 at the same depth, that is, H_{ext} above from the bottom of the system. N_z represents the number of grid blocks to represent the subsurface involved, and one extra hypothetical layer of grid on the top represents the atmosphere (that has much larger volume (i.e., 1,000 times more) than the total pore volume of the subsurface below) that interacts with the air in the upper portion of the soil (i.e., vadose zone). The top layer representing the atmosphere has the pressure value of P_{atm}, while the extraction wells have the pressure value of P_{ext}. Note that the atmospheric pressure (P_{atm}) is fixed and given (as an input), but the P_{ext} value can vary depending on the efficiency of the pumping unit applied to the horizontal wells.

The soil layer has the absolute permeability values of k_x, k_y, and k_z (for simplicity, $k_x = k_y$ and $k_z = k_x/10$) with the porosity of ϕ. There are three relative permeability curves such as k_{rw}, k_{ro}, and k_{rg} involved, and these curves are modified in the presence of surfactants based on the reduced interfacial tension value. Each of the three fluid phases has its own density and viscosity. At its very initial condition (before the leak incident with no oil present), the system is provided with a capillary pressure curve (P_c vs. S_w or P_c vs. S_g) as shown in Figure 5 (together with color contours). Note that in this initial capillary equilibrium, the capillary pressure (P_c) is related to vertical distance (z) linearly (i.e., $P_c = (\rho_w - \rho_g)gz$), but the simulation allowed some waiting time at the beginning to reach its own initial equilibrium which is, of course, a function of system properties.

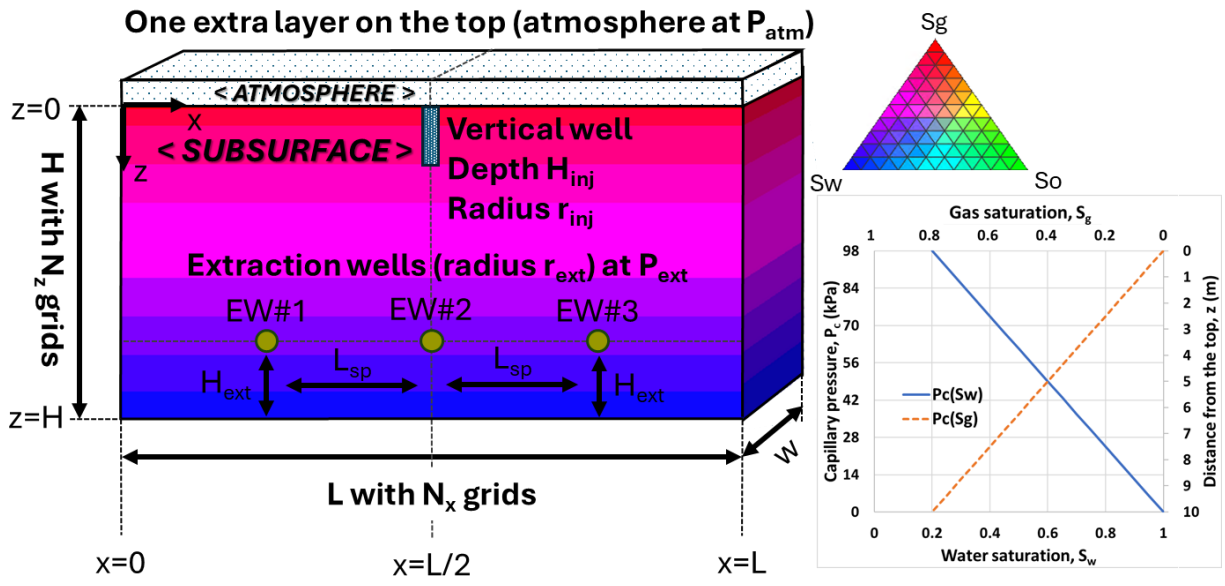

Figure 5 Two-dimensional cross-section for simulation efforts in this study with a vertical injection well and three horizontal extraction wells, showing the initial water saturation and capillary pressure

Table 1 summarizes simulation parameters for gridding, and Table 2 contains information on the petrophysical properties. This study considers a relatively homogenous system before adding more subsurface complexities. This study borrows the three-phase relative permeability curves and related parameter values (Eq. (3) through Eq. (6); Table 2) from the previous studies which deal with remediation treatment sites nearby (6, 14). For the DNAPL contaminants represented by TCE, the properties are obtained from Costanza (10) at near atmospheric conditions as shown in Table 3 together with other components and their related phases.

Table 1. Simulation parameters for gridding

Parameter	Value
Size of the system (L x W x H)	40m x 0.1m x 10m
Number of grid blocks (N_x,N_y,N_z+1)	401, 1, 101
Grid block size	about 0.1m x 0.1m x about 0.1m
Total number of grid blocks	40502

Table 2. Petrophysical properties for simulations

Properties	Value
Porosity (ϕ)	8.0 %

Permeability (k_x, k_y, k_z)	1.0, 1.0, 0.1 darcy
Residual saturation for water, oil, and gas (S_{wr}, S_{or}, S_{gr})	0.2, 0.0, 0.0
End-point water Relative Permeability ($\boldsymbol{k_{rw}^0}$) and exponent (m)	0.79, 1.96
End-point oil relative permeability ($\boldsymbol{k_{ro}^0}$) and exponent (n)	0.9, 2.15
End-point gas relative permeability ($\boldsymbol{k_{rg}^0}$) and exponent (p)	1.0, 2.3
End-point oil relative permeability ($\boldsymbol{k_{rog}^0}$) and exponent (q)	0.9, 2.15
Atmospheric pressure (P_{atm})	101.3 kPa

Note: *1 darcy is about 10^{-12} m^2.*

Table 3. Fluid properties for simulations

Phase (@ Std)	**Density**	**Viscosity**
Water (w/o S)	1070 kg/m^3	1.0 cp
Water (w/ S)	1000	1.0
Oil	1460	0.58
Gas	-	0.02

Component	**M.W.**
Water	0.018 kg/gmole
Surfactant	0.604
TCE	0.1314
Nitrogen	0.028

Note: *Surfactant solution consists of 0.99995 water fraction and 0.00005 surfactant fraction (above its CMC of $5.9x10^{-6}$).*

3. Results

3.1. Events of interest for simulations

This simulation effort consists of two events: i) reproduction of DNAPL leak from the storage tanks and ii) in-situ remediation of the contaminants by introducing surfactant solution from the vertical well (near the top) and extracting fluids from the three horizontal wells (near the bottom). The first event continues for 30 days at the top of the vertical well in Figure 5 (i.e., at the surface level as there is no such a well at the time of leakage) to create a similar volume of underground DNAPL pool from the leak (See Figure 3), that is, about 0.03 m^3 of oil (i.e., oil leak rate $q_o = 1.0 \times 10^{-3}$ m^3/day over the period of 30 days). The first event is followed by the second, which is, 30 days of surfactant imbibition (with active horizontal wells). It must be mentioned that the surfactant injection rate is not an input value – rather, it varies depending on the pressure (P_{ext}) applied at the horizontal wells (therefore the use of "surfactant imbibition rate" is more appropriate in this study rather than "surfactant injection rate"). In other words, the imbibition rate of surfactant solution tends to be higher at lower P_{ext} value (meaning more efficient pumping out). There are no wells during the first event as all wells are added and activated at the beginning of the second event.

The simulation requires some amount of waiting time prior to the first event, for pre-conditioning purposes, so that the system reaches an (near) equilibrium condition in terms of initial saturation (water and air) and capillary pressure. The waiting time of 2.5 days is applied throughout because there is no significant change observed beyond it. In addition, there is an 8-day gap between the first and second events in simulations, with no fluids introduced or extracted, to mimic the duration from the reporting of the accidents and the beginning of the remediation operations in the field. (This gap time can be greater in some field cases, as much as months.)

3.2. Simulation of the first event: DNAPL leakage

The first 30 days of leakage (i.e., Day 1 through Day 30) is simulated, followed by additional 8 days of gap time (i.e., Day 31 through Day 38), as shown in Figure 6. Some key input parameters for CMG simulation (9) are summarized in Table 4.

Table 4. Simulation parameters for the first and second events

Parameter	**Value**
Contaminant leak rate (q_o)	0.001 m^3/d
Extraction well pressure (P_{ext}) drawing surfactant in	0.1, 0.3, 0.5, 0.7 atm (abs)
Interfacial tension (σ_{ow}, w/o S)	32 dyne/cm
Interfacial tension (σ_{ow}, w/ S)	1.0, 0.01 dyne/cm
First Event duration (leak)	30 days
Post-leak duration	8 days

Second event duration (remediation)	30 days
Simulation time step size	4 hours
Extraction well radius (r_{ext})	0.017 m
Vertical well depth and radius (H_{inj}, r_{inj})	2 m, 0.100 m
Horizontal well spacing (L_{sp})	10 m

Note: *1 atm is about 101.3 kPa*.

The DNAPL oil phase (represented by the green color; the color scale consistent with the one in the ternary diagram in Figure 5) is entering the subsurface, from the leak location (at the top center), which is initially occupied by water (blue) and air (red) phases. The results show that the oil phase migrates downward quickly during the first 5 days flowing through the relatively dry media. The oil phase then spreads laterally as the front encounters the media with higher water saturations, forming a large DNAPL pool at the end of Day 30. The shape of the pool captures the DNAPL distribution in Figure 3 qualitatively. During the 8-day gap time with no more oil spill (Day 31 - Day 38), the pool still grows laterally somewhat (especially earlier days) because of downward movement of the oil column above (by the gravity) as well as upward movement of the oil below (by the buoyancy). Although continuing, this process becomes extremely slow after Day 38. Note that the results are symmetrical (across the middle vertical line containing the injection well) as expected.

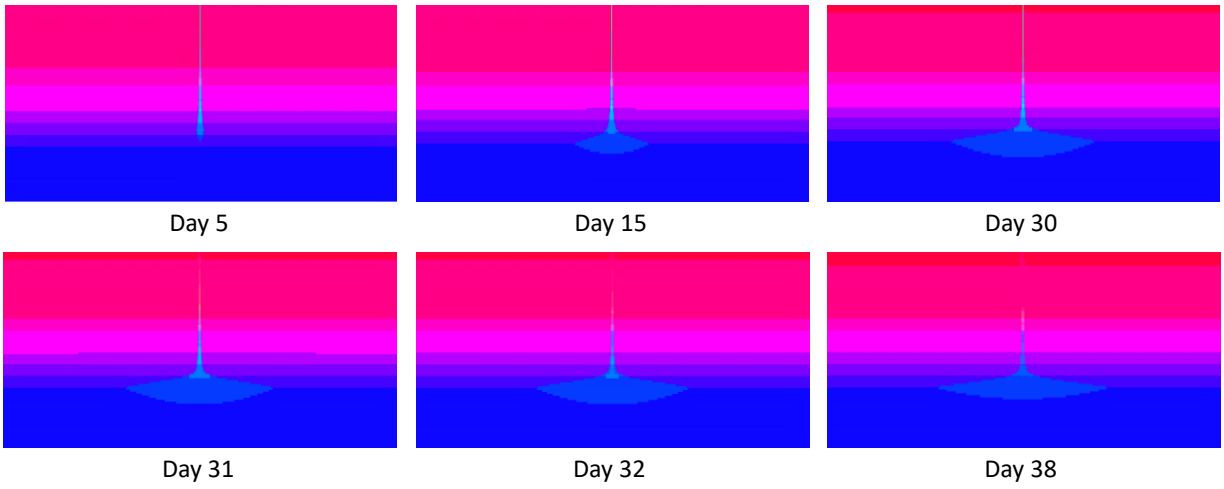

Figure 6 Computer simulation of leak event showing saturation profiles at t = Day 1, Day 15 and Day 30 (during leak) and t = Day 31, Day 32 and Day 38 (post-leak). Note that there are 30 days of oil leak at the rate (q_o) of 0.001 m^3/day followed by 8 days of gap time prior to in-situ remediation

Figure 7 shows the same saturation information as Figure 6 (at the end of Day 5, 15, 30, 31, 32, and 38), but along various (imaginary) vertical scanning lines – lines of 0 m, 0.1 m and 1.0 m away from the middle vertical line. The plots are created such that, at any given time (t) and vertical distance (z), oil saturation (S_o) can be read by the distance from the left (the

green color), while gas saturation (S_g) can be read by the distance from the right (the red color). Therefore, the distance between the two represents water saturation (S_w). (For example, in the uppermost layers near the surface, the distance between the two is about 0.2 which reflects the residual water saturation (S_{wr}) of 0.2.) The results show similar responses to those in Figure 6: During the leak (until Day 30), there is an active downward migration of the oil phase along the middle vertical line that goes with lateral spreading down below, while during the gap time (Day 31 to Day 38), the oil phase tends to concentrate in the middle (around 3 to 6 m depth) gradually forming a plume with the gravity and buoyancy forces.

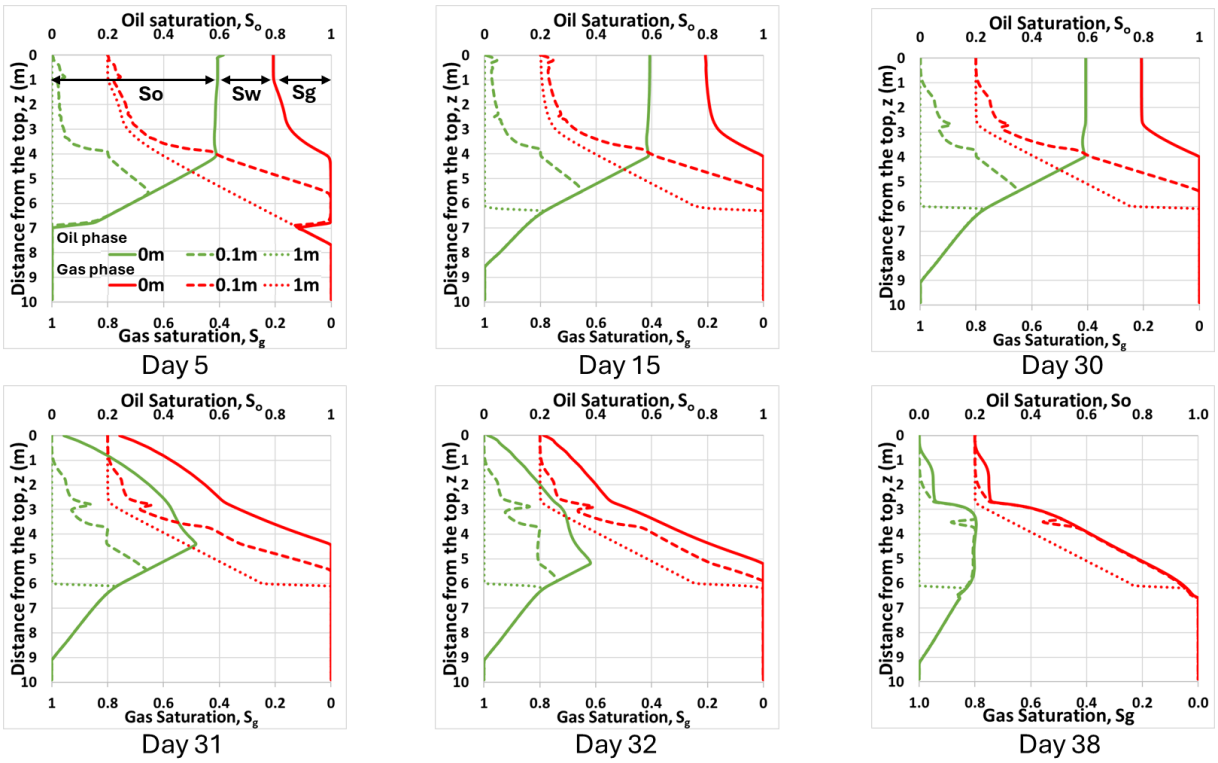

Figure 7 Simulation results of leak scenario showing water, oil and gas saturation (S_w, S_o and S_g) history from the vertical scanning lines of 0 m, 0.1 m, and 1.0 m away from the middle vertical line

3.3. Simulation of the second event: in-situ remediation with surfactant solution

After 30 days of contaminant leak and 8 days of gap time, the remediation process begins by extracting formation fluids from the three horizontal wells drilled. During this operation of suction by pumping fluids out, both air (from the top simulation layer mimicking the atmosphere at the constant pressure of P_{atm}) and surfactant solution (which is always filling the injection well up to the surface level) are drawn into the subsurface, but the surfactant solution has an advantage of migrating downward faster because of its higher density compared to air.

Figure 8 shows the base-case results for surfactant concentration at the outlet pressure (P_{ext}) = 0.1 atm, interfacial tension (σ_{ow}) = 32 dyne/cm, and horizontal well location (H_{ext}) = 1.5 m above from the bottom of the system, following the 38 days of first event (as a result, the second event ranges from Day 39 through Day 68). As the surfactant molecules move downward, they spread and tend to find a preferential path to the middle horizontal well (EW#2) due to the proximity (Day 5 and Day 10). They then travel towards other adjacent wells (EW#1 and EW#3) too, by making a good coverage within the system during the in-situ treatment (i.e., 30 days of surfactant imbibition). The same simulations conducted at σ_{ow} = 1.0 and 0.01 dyne/cm do not show any noticeable differences. Note that σ_{ow} = 32 dyne/cm represents a simple water imbibition scenario (as the interfacial tension is not affected), while σ_{ow} = 1.0 and 0.01 dyne/cm represent the range of σ_{ow} from the lab measurements for Tween-80 at its slightly-below and slight-above critical micelle concentration (CMC). (This non-ionic Tween 80 surfactant has its concentration of 0.1 - 0.2 wt% in the field treatments, far above its CMC (about 0.05 - 0.06 wt%)], with the reported lab-measured interfacial tension of around 0.01 dyne/cm at the CMC value (7, 14).)

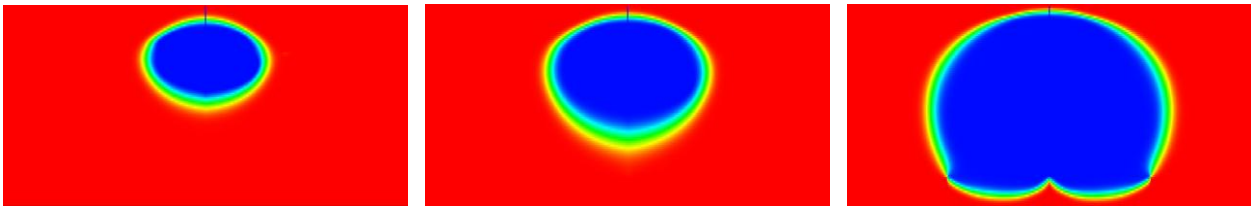

Figure 8 Base case computer simulation of the second event (i.e., 30-day surfactant imbibition) showing the movement of surfactant front (at the end of Day 5, Day 10 and Day 30) – the outlet pressure (P_{ext}) = 0.1 atm, interfacial tension (σ_{ow}) = 32 dyne/cm, and horizontal well location (H_{ext}) = 1.5 m above from the bottom of the system (blue – injected surfactant concentration; red – no surfactant) (10 m well-to-well spacing)

Figure 9 shows the results of oil saturations (which correspond to Figure 8) at three σ_{ow} values of 32, 1.0 and 0.01 dyne/cm. There are some interesting observations to be made. First, if no surfactant chemicals are added (σ_{ow} = 32 dyne/cm), not much change happens during 30

days of imbibition, even with a highly active fluid extraction applied by the horizontal wells. This means that the pressure gradient created by pumping itself is not large enough to mobilize oil blobs trapped by the capillary force (the same can be explained by the dimensionless capillary number), and thus the operation with no surfactants is unlikely to be successful in terms of DNAPL removal. Second, with σ_{ow} = 1.0 and 0.01 dyne/cm (i.e., enough surfactant chemicals added), the process can remove DNAPLs meaningfully at its reduced capillary pressure environment or at its improved capillary number environment. There is no significant difference between the two σ cases. Third and last, with the extraction well pressure of P_{ext} = 0.1 atm and the well-to-well spacing of 10 m, some DNAPLs (near the wells) are sucked into the extraction wells and produced easily, while other DNAPLs (away from the wells) migrate further down to make the recovery even more difficult. This may require follow-up in-situ remediation actions such as using biological agents in the future.

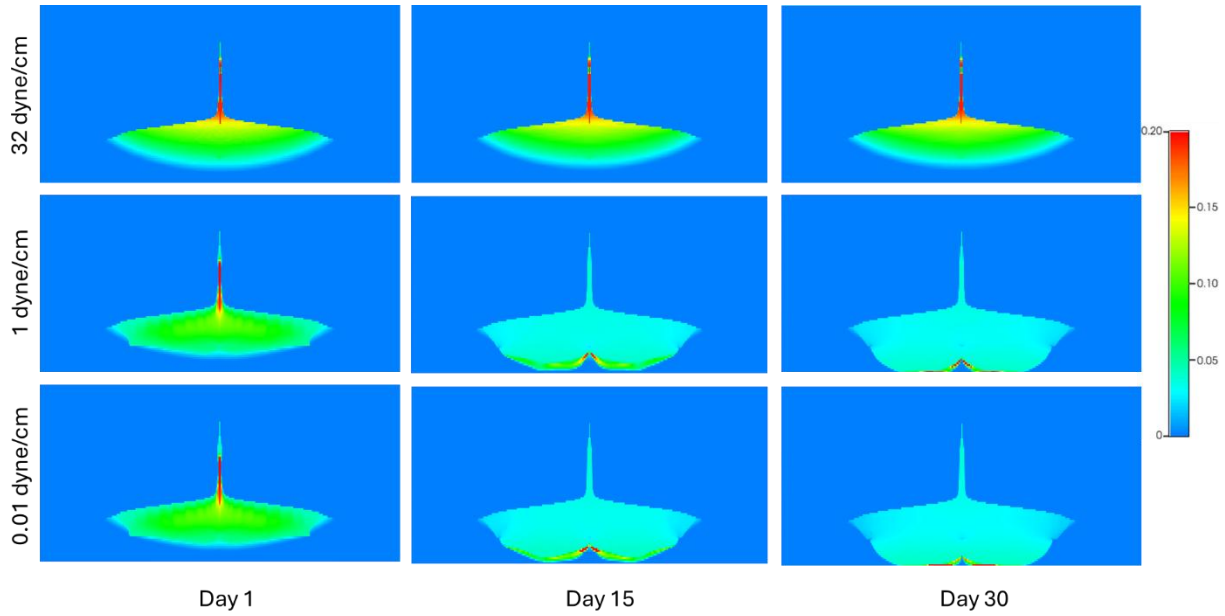

Figure 9 Computer simulation of 30-day surfactant imbibition event showing oil saturations (at the end of Day 1, Day 15 and Day 30 with P_{ext} = 0.1 atm and H_{ext} = 1.5 m) at the interfacial tension (σ_{ow}) of 32, 1.0, and 0.01 dyne/cm (10 m well-to-well spacing)

Figure 10 shows the cumulative oil recovery (which corresponds to Figure 8 and Figure 9) at the three σ_{ow} values of 32, 1.0 and 0.01 dyne/cm during the same 30-day remediation period. The results are consistent with the observations from Figure 9, including negligible oil recovery when σ_{ow} = 32 dyne/cm (no surfactant); meaningful recovery when σ_{ow} = 1.0 and 0.01 dyne/cm; and EW#2 as a main player compared to EW#1 and EW#3. It is interesting to find that most of the recovery from the middle well (EW#2) is made within about 5 days of the remediation process. When compared with the actual in-situ remediation operations (σ_{ow} = 0.01 dyne/cm, H_{ext} = 1.5 m), the simulation results successfully reproduce the trend qualitatively – a noticeable recovery in the first 7 days and a follow-up additional recovery until the end of 30 days of operations, resulting in around 30 - 40 % NAPL recovery. The

simulation results are also consistent with field data in that there was no recognizable amount of DNAPL recovery during the last 30 days (i.e. second month of operation).

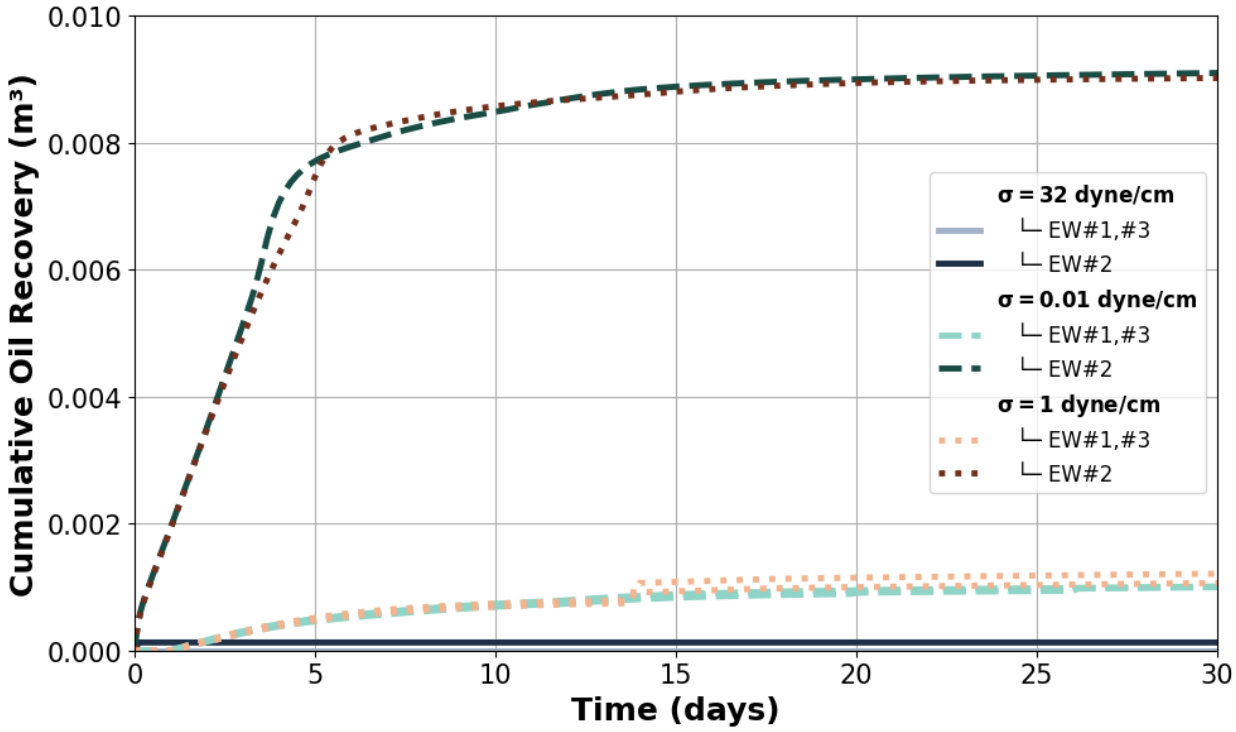

Figure 10 Cumulative oil recovery from three horizontal wells (EW#1, EW#2 and EW#3) at the interfacial tension (σ_{ow}) of 32, 1.0, and 0.01 dyne/cm over 30 days of surfactant imbibition (Day 39 through Day 68) (P_{ext} = 0.1 atm and H_{ext} = 1.5 m). Note that the total oil spill volume is 0.03 m^3 (10 m well-to-well spacing)

In addition to these base-case scenarios (Figure 8 through Figure 10), other scenarios are investigated by changing the horizontal extraction well location (H_{ext}) - 3 meters and 5 meters from the bottom (rather than 1.5 m) as shown in Figure 11 through Figure 13 and in Figure 14 through Figure 16, respectively. The general responses can be listed as follows: First, surfactant chemicals migrate downwards, reaching the elevation slightly lower than the horizontal wells, but not significantly lower than that (See Figure 11 and Figure 14). Second, because of the first on the coverage of surfactant molecules, any DNAPL contaminants located below the horizontal wells cannot be contacted by the surfactant solution and have a hard time being mobilized and recovered (See Figure 12 and Figure 15). This is an important finding when it comes to deciding the elevation of the horizontal wells to be drilled. And lastly, the oil recovery values at higher H_{ext} (or, further above from the bottom of the system) become lower, and the meaningful recovery only occurs at earlier time (within 3-4 days when H_{ext} = 3 m; within 1-2 days when H_{ext} = 5 m; see Figure 13 and Figure 16).

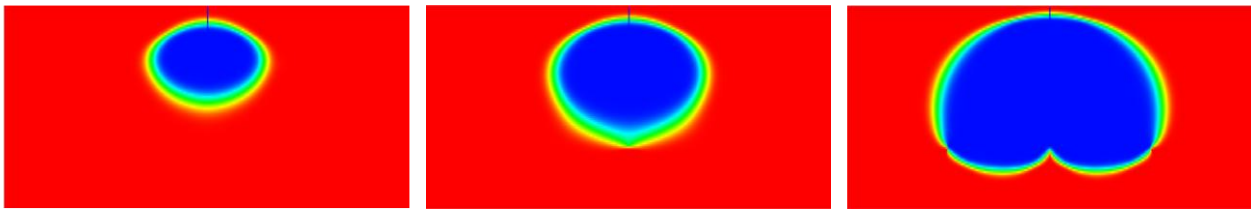

Figure 11 Computer simulation of the second event (i.e., 30-day surfactant imbibition) showing the movement of surfactant front (at the end of Day 5, Day 10 and Day 30) when the horizontal well location (H_{ext}) = 3 m from the bottom (rather than 1.5 m). All other parameters are the same as those in Figure 8

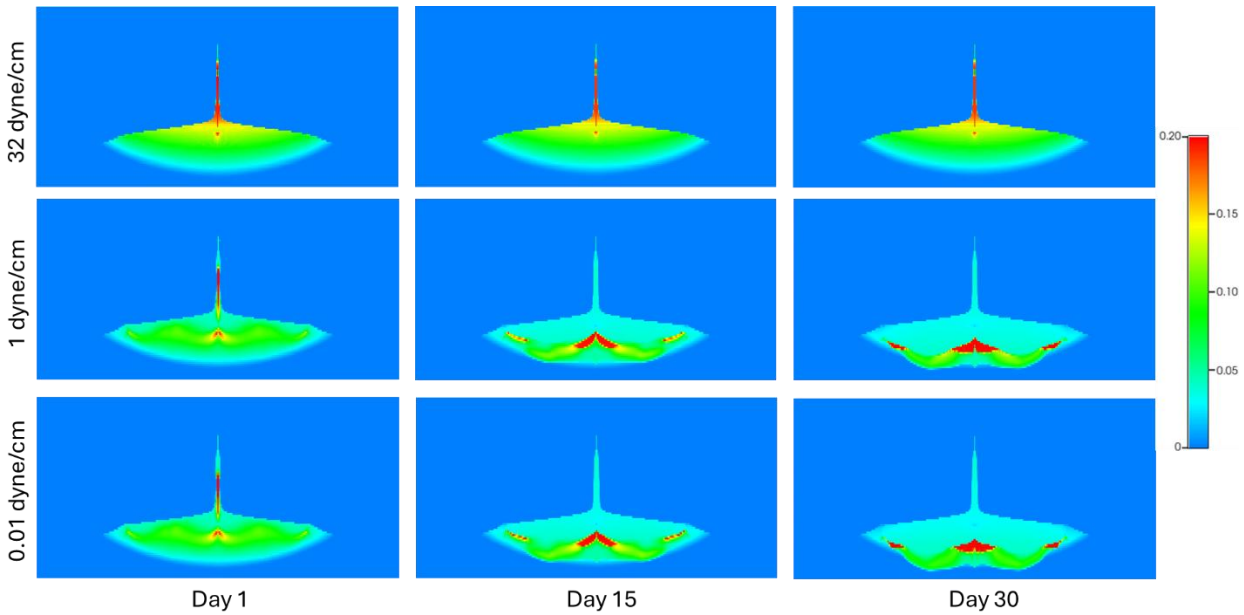

Figure 12 Computer simulation of 30-day surfactant imbibition event showing oil saturations when the horizontal well location (H_{ext}) = 3 m from the bottom (rather than 1.5 m). All other parameters are the same as those in Figure 9

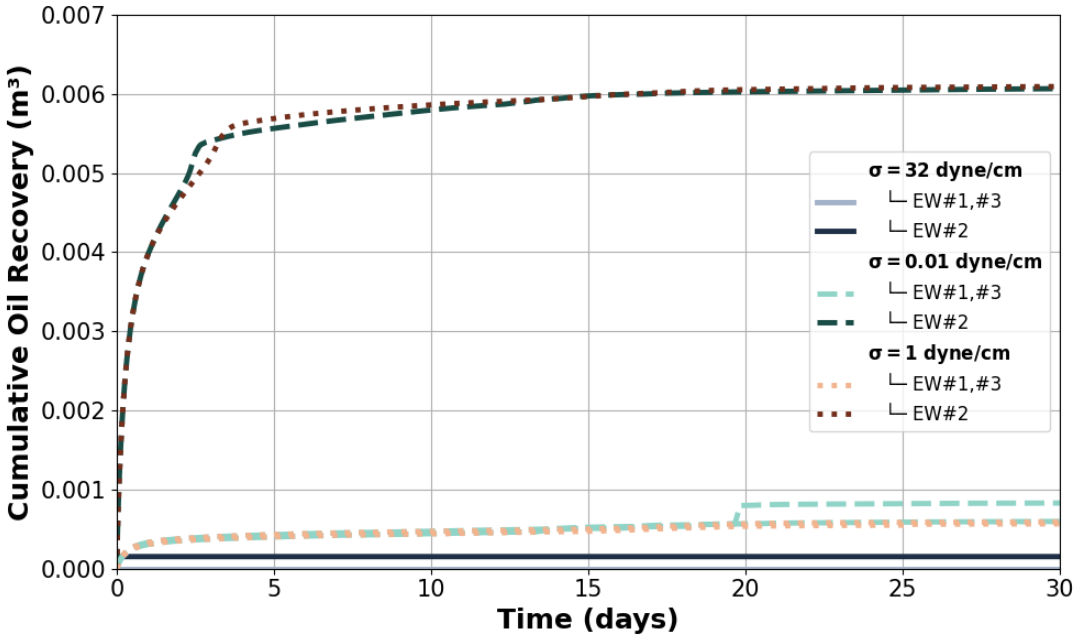

Figure 13 Cumulative oil recovery from three horizontal wells (EW#1, EW#2 and EW#3) when the horizontal well location (H_{ext}) = 3 m from the bottom (rather than 1.5 m). All other parameters are the same as those in Figure 10

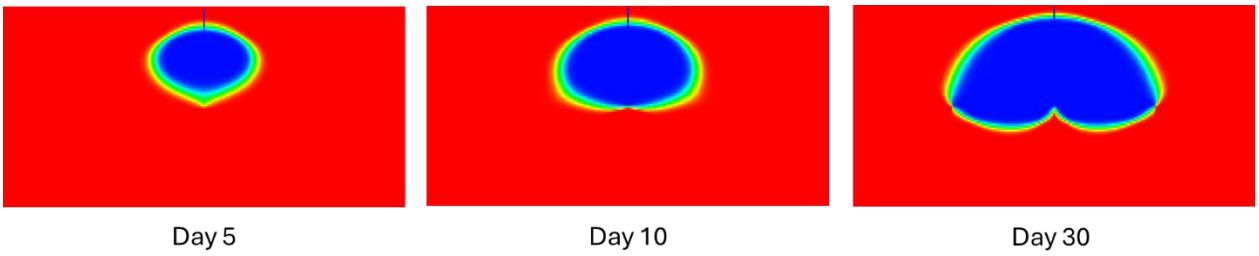

Figure 14 Computer simulation of the second event (i.e., 30-day surfactant imbibition) showing the movement of surfactant front (at the end of Day 5, Day 10 and Day 30) when the horizontal well location (H_{ext}) = 5 m from the bottom (rather than 1.5 m). All other parameters are the same as those in Figure 8

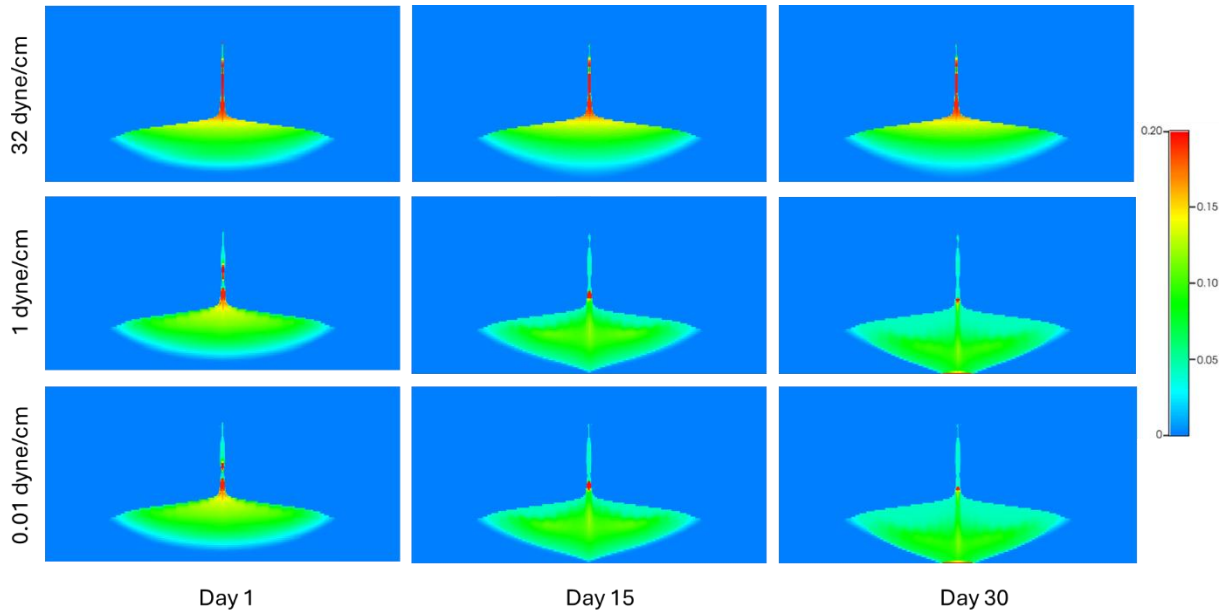

Figure 15 Computer simulation of 30-day surfactant imbibition event showing oil saturations when the horizontal well location (H_{ext}) = 5 m from the bottom (rather than 1.5 m). All other parameters are the same as those in Figure 9

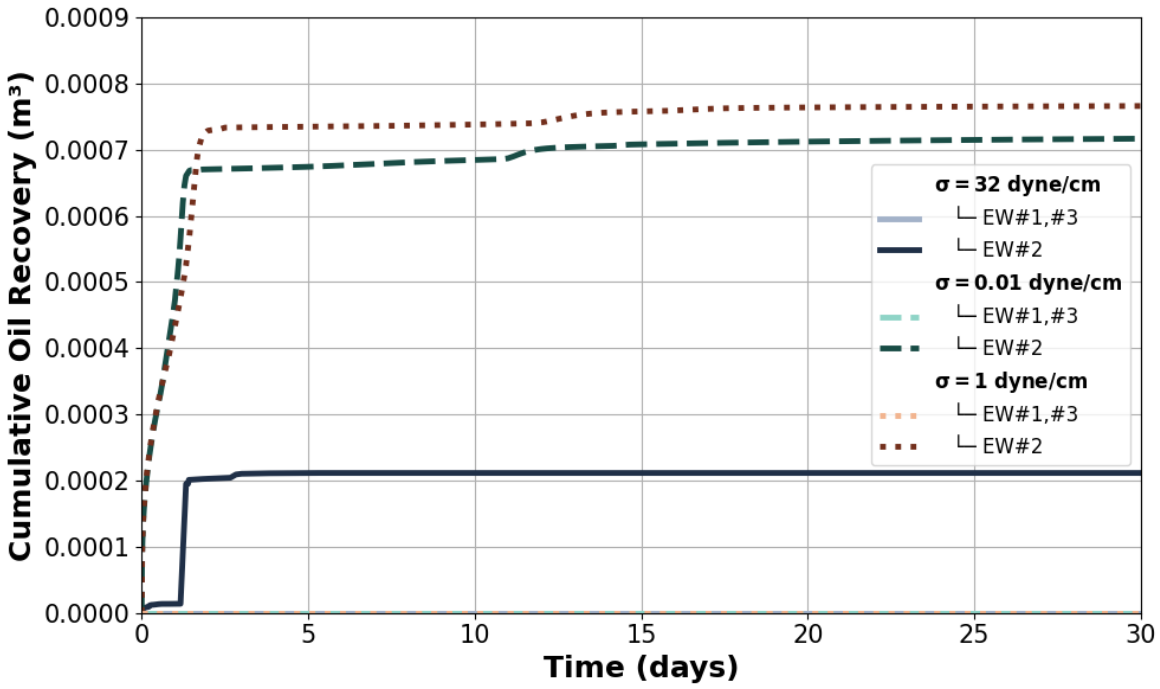

Figure 16 Cumulative oil recovery from three horizontal wells (EW#1, EW#2 and EW#3) when the horizontal well location (H_{ext}) = 5 m from the bottom (rather than 1.5 m). All other parameters are the same as those in Figure 10

The results described so far (Figure 8 through Figure 16) are the cases when the pumping system is well designed and applied, as intended, with a low value of outlet pressure (P_{ext} = 0.1 atm) attainable. Separate field testing results show that pumping formation fluids out efficiently from the horizontal wells is not really a concern as long as the horizontal wells are positioned below the groundwater level (as shown in this study; see Figure 4). It can be inefficient, however, if the wells are positioned above the groundwater level and pump cavitation deteriorates pump performance. As such, the simulations are repeated at various P_{ext} values, as a part of sensitivity analysis, including P_{ext} = 0.3, 0.5, and 0.7 atm (Note that P_{ext} is expressed in terms of *absolute pressure* such that P_{ext} = 0.0 atm means the case of perfect vacuum obtained while P_{ext} = 1.0 atm means wells drilled but with no pumping performed). The results summarized in Figure 17 and Table 5 show that the recovery efficiency decreases with increasing P_{ext} values, demonstrating the importance of the pumping unit in the field. Note that, in all scenarios investigated with DNAPL volume of about 0.03 m^3, the maximum recovery is about 36 - 37 % which occurs when the outlet pressure (P_{ext}) = 0.1 atm, horizontal well location (H_{ext}) = 1.5 m, and interfacial tension (σ_{ow}) = 1.0 or 0.01 dyne/cm. Simple water imbibition (with no surfactant) cases do not work as they show negligible recovery values (mostly less than 0.7 %).

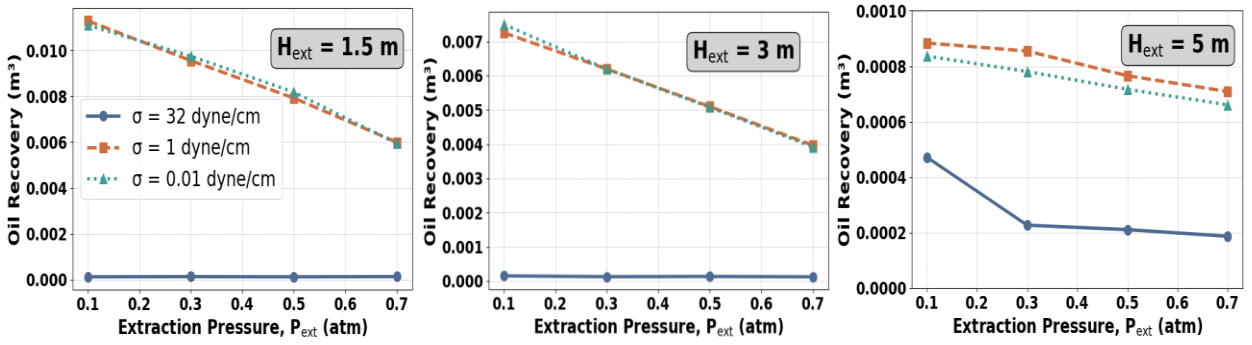

(a) (b) (c)

Figure 17 Summary of simulation results from 30-day surfactant imbibition event at various σ_{ow} and P_{ext} values: (a) H_{ext} = 1.5 m, (b) H_{ext} = 3.0 m and (c) H_{ext} = 5.0 m. (Total oil spill volume is about 0.03 m^3)

Although not shown here, additional simulations are performed to investigate the effect of well-to-well spacing (L_{sp}). The two cases recovering about 36 to 37 % of oil in Table 5 (L_{sp} = 10 m) can be improved up to the range of about 52 to 53 % (i.e., 0.0156 to 0.016 m^3) by reducing L_{sp} down to 3 to 5 m.

Table 5. A summary of recovery and recovery efficiency from all scenarios investigated

Height from bottom, H_{ext} [m]	σ_{ow} = 32 [dyne/cm]	σ_{ow} = 1 [dyne/cm]	σ_{ow} = 0.01 [dyne/cm]	Extraction pressure, P_{ext} [atm]
1.5	0.000135 (0.45%)	**0.011024 (36.7%)**	**0.011050 (36.8%)**	0.1
3	0.000213 (0.71%)	0.007239 (24.1%)	0.007368 (24.6%)	
5	0.000567 (1.9%)	0.000879 (2.9%)	0.000888 (3.0%)	
1.5	0.000133 (0.44%)	0.009550 (31.8%)	0.009744 (32.5%)	0.3
3	0.000129 (0.43%)	0.006194 (20.6%)	0.006193 (20.6%)	
5	0.000227 (0.76%)	0.000855 (2.9%)	0.000781 (2.6%)	
1.5	0.000137 (0.46%)	0.007917 (26.4%)	0.008178 (27.3%)	0.5
3	0.000150 (0.5%)	0.005097 (17.0%)	0.005075 (17.0%)	
5	0.000211 (0.70%)	0.000766 (2.6%)	0.000717 (2.4%)	
1.5	0.000135 (0.45%)	0.005995 (20.0%)	0.005941 (19.8%)	0.7
3	0.000125 (0.42%)	0.003965 (13.2%)	0.003919 (13.1%)	
5	0.000187 (0.62%)	0.000709 (2.4%)	0.000661 (2.2%)	

4. Discussions

4.1.Follow-up research activities

The main outcome of this study reveals the feasibility of in-situ vertical-well surfactant-imbibition remediation methods with active horizontal wells extracting formation fluids down below. The process, however, requires an optimization study that includes many design parameters (as demonstrated in this study) such as petrophysical properties of the subsurface of interest, fluids associated, injection and extraction methods, well-to-well spacing, among many.

One extension of this technology is using a mixture of air and surfactant solution (potentially creating foams) for blocking and diverting purposes, as conceptually presented by Cepeda-Salgado et al. (7) as shown in Figure 18. This particular technology requires an injection of the fluid mixture into the adjacent wells so that the subsequent surfactant solutions imbibed are directed into the middle well.

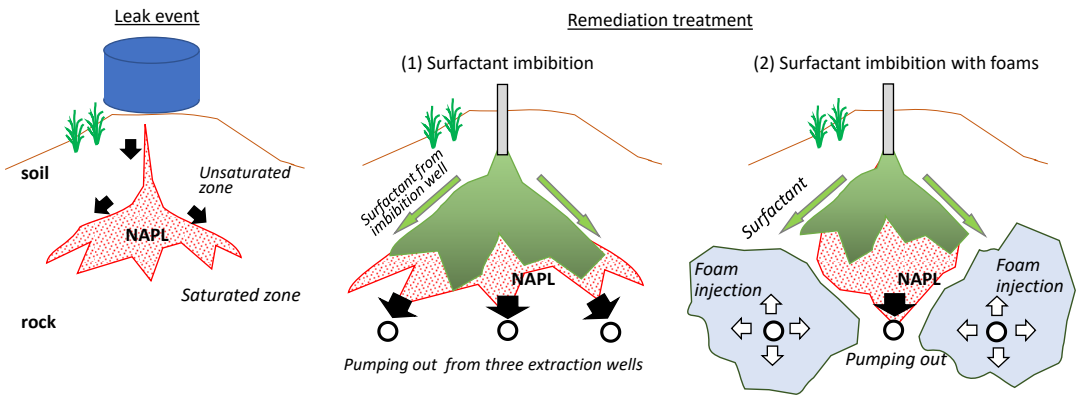

Figure 18 Conceptual drawing of enhanced horizontal well treatment with blocking and diverting foams (following Cepeda-Salgado et al. 2023)

Such an activity also motivates three-dimensional simulation work – whether it is only with surfactant solutions or fluid mixtures. Figure 19 shows an example during the infant stage of the work.

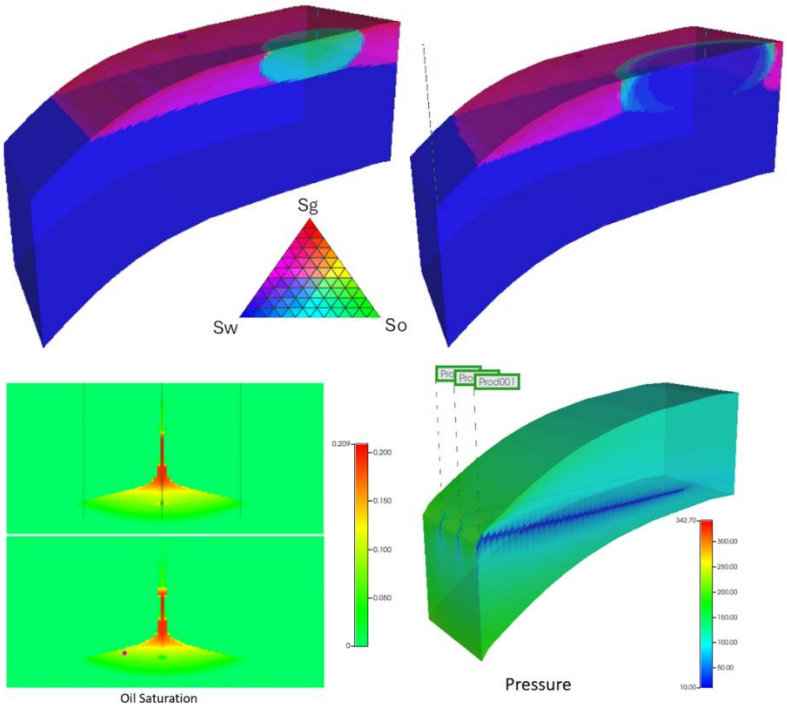

Figure 19 Some initial test runs for 3D simulations: oil spill followed by imbibition of surfactant solutions (top) and migration of oil and pressure distribution (bottom)

4.2.Understanding key mechanisms by using dimensionless number

The results presented in this study show that the recovery of DNAPL pollutants is impacted by 4 major parameters – well-to-well spacing between horizontal extraction wells (L_{sp}), horizontal well elevation (H_{ext}), horizontal well pressure (P_{ext}), and interfacial tension between oil and water (σ_{ow}). Although the first two (L_{sp} and H_{ext}) are related to the sweep efficiency in a multi-dimensional space, the second two (P_{ext} and σ_{ow}) are related to the fundamental pore-scale displacement mechanisms associated with mobilization of oil blob which requires capillary pressure (P_c) greater than the capillary entry pressure (P_{ce}). (Note that P_{ce} is defined as $P_{ce} = 2\sigma_{ow}/r_{th}$, where σ_{ow} and r_{th} being the interfacial tension and pore throat radius, respectively.) See Lake (19) for more details.

Figure 20 depicts the concept of capillary entry pressure (left) that works as the capillary-pressure barrier for a non-wetting phase oil blob to overcome at the pore throat to move into the next pore body. A similar behavior happens for a NAPL droplet (at the boundary between the subsurface and horizontal well) that is about to be produced (right). For instance, the pressure acting on the droplet by the continuous column of the wetting-phase water through the pore network above can be simplified roughly with $[P_{atm} + \rho_w g(H - H_{ext})]$, the pressure in the horizontal well is P_{ext}, and thus the capillary pressure at the bottom of the droplet is about $[P_{atm} + \rho_w g(H - H_{ext})] - P_{ext}$, which can be compared with P_{ce}. Therefore, the condition for the NAPL droplet to be produced is as follows:

$$[P_{atm} + \rho_w g(H - H_{ext})] - P_{ext} > \frac{2\sigma_{ow}}{r_{th}} \quad \text{or} \quad (11)$$

$$Dimensionless\ number\ F = \frac{[P_{atm} + \rho_w g(H - H_{ext})] - P_{ext}}{\frac{2\sigma_{ow}}{r_{th}}} > 1 \quad (12)$$

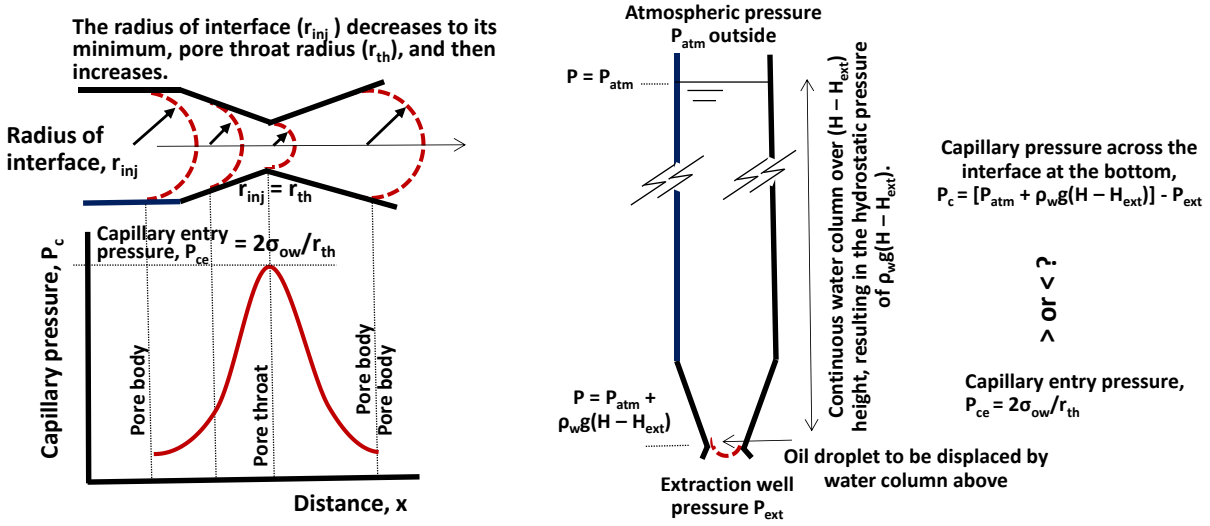

Figure 20 Fundamental displacement mechanisms and associated dimensionless number concept

In order to test if this dimensionless number F (which is $\{ [P_{atm} + \rho_w g(H - H_{ext})] - P_{ext} \} / [2\sigma_{ow}/r_{th}]$ comparing the two capillary pressure values) governs the displacement process, additional

calculations are performed to come up with Figure 21 – contours of the dimensionless number F as a function of P_{ext} and σ. Note that P_{atm} = 101.1 kPa (or 1 atm), ρ_w = 1000 kg/m^3, g = 9.81 m/s^2, (H – H_{ext}) = 8.5 m (i.e., 10.0 m – 1.5 m), and $r_{th} \cong \sqrt{k_z} = \sqrt{0.1k_x} \cong 1.8 \times 10^{-7}$ m (i.e., $k_z \cong (0.1 \times 10^{-12})$ m^2 and $\pi r_{th}^2 \cong 10^{-13}$ m^2) in these calculations. The results clearly show that P_{ext} and σ_{ow} values are major parameters to govern the pore-scale event of field remediation treatments – the lower the P_{ext} and σ_{ow} are, the higher the oil recovery becomes, if other conditions remain identical. The contours also explain why the case of σ_{ow} = 0.01 or 1.0 dyne/cm is much more efficient than the case of σ_{ow} = 32 dyne/cm, in terms of mobilizing the NAPL droplets originally trapped by the capillary force.

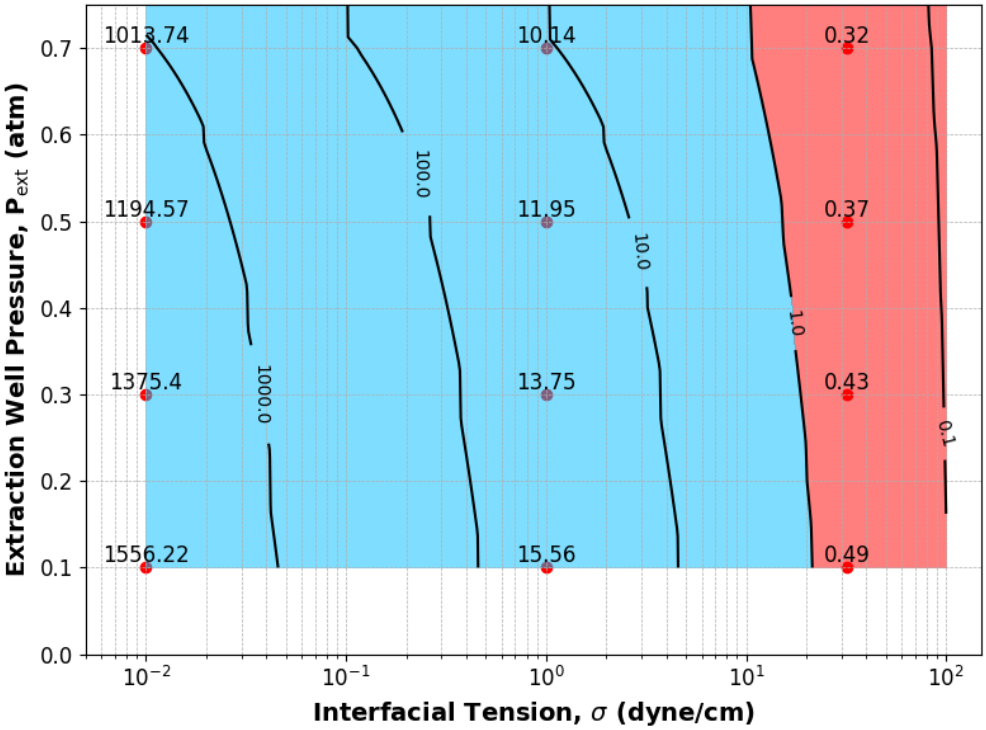

Figure 21 Evaluation of displacement outcomes in this study by using the dimensionless number F (if F > 1.0, the NAPL blob can then be mobilized and produced) (Note that 1 atm is about 101.1 kPa.)

According to Lake (19; Chapter 6), the overall volumetric sweep efficiency consists of microscopic efficiency (governed by pore-scale event) and macroscopic efficiency (governed by both areal and vertical sweep), i.e., overall volumetric sweep efficiency = microscopic efficiency x macroscopic efficiency, where macroscopic efficiency = areal sweep x vertical sweep. The dimensionless number F represents the microscopic efficiency which can be controlled in this study to improve the recovery in the field operations (for example, choosing surfactant chemicals (i.e., types and concentrations) to achieve a sufficient level of interfacial tension reduction which allows trapped oil blobs to be mobilized at certain hydrostatic pressure conditions. In the meantime, this study makes no efforts to

control or modify the macroscopic efficiency. As the properties of surfactant solution is similar to those of water (other than interfacial tension reduction), the sweep efficiency is almost identical for the two cases. The next phase of study, in fact, is to deal with the macroscopic efficiency by injecting air and surfactant solutions (potentially creating foams) as a sequel.

4.3. Other field-scale challenges

4.3.1. Uncertainty of subsurface heterogeneity

The modeling and simulation efforts in this study assume that the subsurface of interest is relatively homogeneous with uniform petrophysical properties, which is never true and clearly one of the major limitations associated with underground geological settings. This section extends the work to conduct sensitivity analysis by performing additional simulations, taking natural compaction into account (as an example of subsurface heterogeneity) – in simulations, such a nature can be captured with the absolute permeability decreasing with depth (z).

Figure 22 shows oil saturation distributions when the absolute permeability decreases with depth linearly or exponentially, in contrast with no change in permeability (See the base-case scenario (Figure 9 and Figure 10) at σ_{ow} = 1.0 dyne/cm; all other parameters are kept identical including the porosity value, therefore the pore volume of the system remains the same in all three cases). In both linear and exponential cases, $k_x = k_y$ = 1.0 darcy at z = 0 m (top) and $k_x = k_y$ = 0.5 darcy at z = 10 m (bottom) – in the case of exponential decrease, the coefficient of -0.069 is used (i.e., exp[-0.069z]). The 30-day recovery factors in both cases are similar (about 36.6 %) to that of the base case (36.7 %; see Table 5). The only noticeable difference is that (i) the oil recovery slows down because of reduced permeability and (ii) the edge wells play slightly more roles in terms oil production due to the delay in vertical migration. These simulation results imply that the results of this study can be reliable unless there is a significant level of subsurface heterogeneity. (Nevertheless, there is no doubt that subsurface heterogeneity plays a key role in in-situ remediation treatments.)

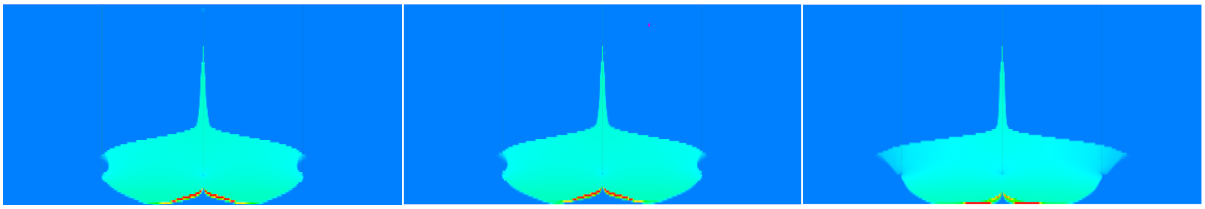

Figure 22 Evaluation of permeability reduction with depth: linear decrease vs. exponential decrease vs. no change (base case in Figure 9 at σ_{ow} = 1.0 dyne/cm) at the end of 30-day surfactant imbibition

While this new remediation approach shows promising simulation results, the applicability of the methodology across different soil/NAPL types and subsurface heterogeneities should

not be forgotten. In the case of this particular site, months-long site investigations were conducted prior to the in-situ remediation, including soil properties (sand/silt/clay contents, water content, texture, pH, CEC), NAPL properties (composition, areal and vertical distribution), groundwater properties (pH, composition, hydrostatic pressure gradient profiling, flow direction), resistivity log for cross-sectional analysis, and monitoring and mapping (GPS and plane surveying).

4.3.2. Field operation facilities to handle produced fluids and recycle surfactants

Surfactant loss and chemical cost are important components when it comes to the economics of field remediation operations. Two different types of efforts were made during the designing phase – i) selection of surfactant (in this case, non-ionic Tween 80 surfactant solution (0.1 - 0.2 wt%) from the laboratory surfactant screening tests) that can reduce the interfacial tension effectively (as low as 0.01 dyne/cm) and, at the same time, exhibit low critical micelle concentration (about 0.05 - 0.06 wt% for the Tween 80 chosen), and ii) use of remediation facilities that allow the surfactant molecules to be recycled (i.e., collecting produced fluids from extraction wells – separating and recycling surfactant solution – pumping it to the top of the hill to be re-distributed to the nearby vertical imbibition wells).

Figure 23 shows the examples of field facilities to handle produced fluids and recycle surfactant solutions during the operation. Presented below are the pumping units (for both injection and extraction lines), separation, filtration, treatment and storage units, fluid distribution system for surfactant imbibition (vertical wells on the hill top), and control system.

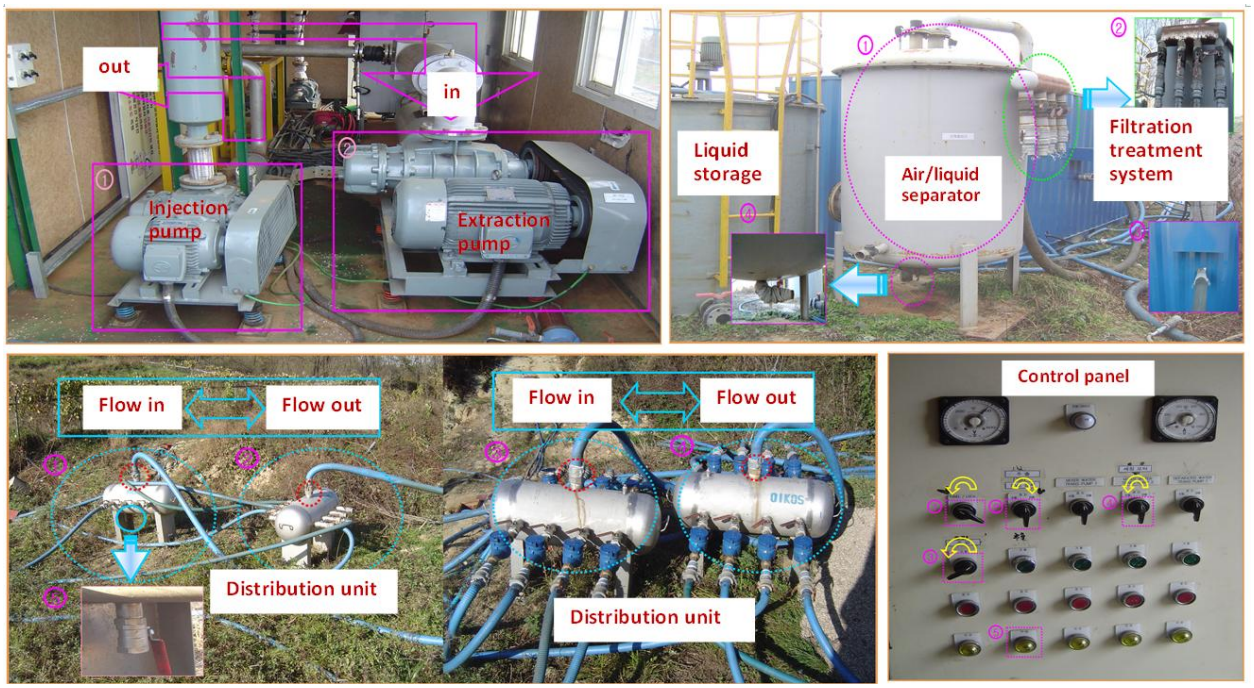

Figure 23 Operation facilities to handle produced fluids and recycle surfactant solutions

The entire project term was 2 years consisting of 3 main phases – Phase 1 for site investigation (soil, contaminant, NAPL distribution, subsurface system, etc.) and facilities set-up (well construction, fluid sampling and treatment, pumping and circulation/distribution unit); Phase 2 for in-situ remediation (about 30 - 40 % recovery, similar to that shown in this study), and Phase 3 for follow-up treatments (additional in-fill vertical wells drilled to improve the recovery up to 90 % (using the same surfactants), and then bio-remediation (injection of biological agents together with the surfactant solutions) for the remaining NAPL treatments. The site was successfully remediated eventually, showing the contaminant level (both in groundwater and soils) below the standard as requested.

5. Summary and Conclusions

This study investigates an innovative technology of in-situ vertical-well surfactant-imbibition remediation methods, with active horizontal wells extracting formation fluids down below. The two-dimensional computer simulation deals with a representative vertical segment (40 m x 10 m x 0.1 m) with the initial oil spill volume of 30 liters (or, 0.030 m^3) from the leak event and follow-up remediation process in various operation scenarios. The conclusions can be summarized as follows:

-. The use of 30-day in-situ surfactant-imbibition remediation methods in conjunction with horizontal extraction wells is shown to be a potentially efficient means of treating DNAPL contaminants, as it improves the recovery efficiency from almost negligible (using water) to

36 - 37 % (using surfactant solutions) at the horizontal well-to-well spacing of 10 meters. Although two-dimensional, the simulation efforts in this study successfully reproduce the range of recovery efficiency shown in the field trials (that is about 30 - 40 %). The simulation results show that even higher recovery efficiency is possible (52 - 53 %) if the well-to-well spacing is reduced down to 3 - 5 meters.

-. For the design evaluated (one injection well at the top and three extraction wells (8.5 m depth and 10 m spacing), the efficiency of pumping units (at the outlet connected to the horizontal wells) and the level of interfacial tension reduction by surfactant chemicals are two crucial parameters. The outlet pressure value of (as low as) 0.1 atm and the interfacial tension value of (as low as) 0.01 - 1.0 dyne/cm are needed to achieve the recovery efficiency of 36 - 37 %. This finding is well supported by the microscopic sweep efficiency explained with the dimensionless number F in this study.

-. In addition to the microscopic sweep efficiency controlled by surfactant imbibition (and analyzed by the dimensionless number F) in this study, follow-up research activities are to be conducted to evaluate the use of air-water mixture (potentially creating foams, if surfactant molecules present) as a means of improving macroscopic sweep efficiency. All of these efforts should be combined with three-dimensional modeling and simulations ultimately to guide field-scale treatments.

Author Contributions

Betty Cepeda-Salgado: conceptualization, data curation, formal analysis, methodology, visualization, writing – original draft. Gyu S. Lee: conceptualization, investigation, resources. Frank Tsai: resources, supervision, writing – review & editing. Seung I. Kam: conceptualization, formal analysis, resources, supervision, visualization, writing – review & editing.

Acknowledgement

This study has been performed by generous supports (both financial and non-financial) from the Craft and Hawkins Department of Petroleum Engineering and Rural Research Institute in Korea Rural Community Corporation (KRCC). Another special appreciation goes to Professor Karsten Thompson at Louisiana State University for his comments, remediation engineers in KRCC for field and lab data, and Computer Modeling Group for simulation support.

Conflicts of Interest

There are no conflicts of interest to declare.

References

1. Allouche, E. N., Ariaratnam, S. T., & Biggar, K. W. (1998). Environmental remediation using horizontal directional drilling: Applications and modeling. Practice Periodical of Hazardous, Toxic, and Radioactive Waste Management, 2(3), 93–99. https://doi.org/10.1061/(ASCE)1090-025X(1998)2:3(93)
2. Bortone, I., Erto, A., Di Nardo, A., Santonastaso, G. F., Chianese, S., & Musmarra, D. (2020). Pump-and-treat configurations with vertical and horizontal wells to remediate an aquifer contaminated by hexavalent chromium. Journal of Contaminant Hydrology, 235, 103725. https://doi.org/10.1016/j.jconhyd.2020.103725
3. Brooks, R. H., & Corey, A. T. (1966). Properties of porous media affecting fluid flow. Journal of the Irrigation and Drainage Division, 92(2), 61–88. https://doi.org/10.1061/jrcea4.0000425
4. Brown, C. L., Delshad, M., Dwarakanath, V., Jackson, R. E., Londergan, J. T., Meinardus, H. W., McKinney, D. C., Oolman, T., Pope, G. A., & Wade, W. H. (1999). Demonstration of surfactant flooding of an alluvial aquifer contaminated with dense nonaqueous phase liquid. In ACS Symposium Series (Vol. 725, pp. 64–85). https://doi.org/10.1021/bk-1999-0725.ch006
5. Brown, C. L., Pope, G. A., Abriola, L. M., & Sepehrnoori, K. (1994). Simulation of surfactant-enhanced aquifer remediation. Water Resources Research, 30(11), 2959–2977. https://doi.org/10.1029/94WR01458
6. Cepeda-Salgado, B., Fleifel, H., Lee, G. S., & Kam, S. I. (2022). A simulation study of in-situ NAPL remediation treatment by using surfactant and foam processes in a military base South Korea. Journal of Contaminant Hydrology, 247, 103982. https://doi.org/10.1016/j.jconhyd.2022.103982
7. Cepeda-Salgado, B., Lee, G. S., Gupta, I., Willson, C., & Kam, S. I. (2023). Surfactant/foam processes in shallow subsurface remediation: Evaluation of foams as a blocking agent. Transport in Porous Media, 149(3), 709–732. https://doi.org/10.1007/s11242-023-01980-y
8. Childs, J., Acosta, E., Annable, M. D., Brooks, M. C., Enfield, C. G., Harwell, J. H., Hasegawa, M., Knox, R. C., Rao, P. S. C., Sabatini, D. A., Shiau, B., Szekeres, E., & Wood, A. L. (2005). Field demonstration of surfactant-enhanced solubilization of DNAPL at Dover Air Force Base, Delaware. Journal of Contaminant Hydrology, 82(1–2), 1–22. https://doi.org/10.1016/j.jconhyd.2005.08.008
9. Computer Modeling Group Ltd. (CMG). (2023). STARS, BUILDER user guide. CMG.
10. Costanza, J. (2005). Degradation of tetrachloroethylene and trichloroethylene under thermal remediation conditions (Doctoral dissertation, Georgia Institute of Technology). https://smartech.gatech.edu/bitstream/1853/7485/1/costanza_jed_200512_phd.pdf.pdf
11. Delshad, M., Pope, G., & Sepehrnoori, K. (1996). A compositional simulator for modeling surfactant enhanced aquifer remediation: 1. Formulation. Journal of Contaminant Hydrology, 23(4), 303–327. https://doi.org/10.1016/0169-7722(95)00106-9

12. Ellis, W., Payne, J., & McNabb, G. (1985). Treatment of contaminated soils with aqueous surfactants (EPA/600/2-85/129). Hazardous Waste Engineering Research Laboratory, U.S. Environmental Protection Agency.
13. Feng, C., Kong, L., Wang, Y., Gu, A., & Huang, X. (2023). Testing of a novel multi-branch horizontal well remediation technology for in situ remediation of contaminated soil and groundwater. Journal of Environmental Management, 344, 118583. https://doi.org/10.1016/j.jenvman.2023.118583
14. Fleifel, H., Izadi, M., Park, S., Gupta, I., Lee, G., & Kam, S. I. (2020). Shallow subsurface environmental remediation by using tracer–surfactant–foam processes: History-matching and performance prediction. Transport in Porous Media, 134(3), 565–592. https://doi.org/10.1007/s11242-020-01458-1
15. Fountain, J. C., Klimek, A., Beikirch, M. G., & Middleton, T. M. (1991). The use of surfactants for in situ extraction of organic pollutants from a contaminated aquifer. Journal of Hazardous Materials, 28(3), 295–311. https://doi.org/10.1016/0304-3894(91)87081-C
16. Holzmer, F. J., Pope, G. A., & Yeh, L. (Eds.). (2000). Surfactant-enhanced aquifer remediation of PCE-DNAPL in low permeability sands. In Proceedings of the Second International Conference on Remediation of Chlorinated and Recalcitrant Compounds. Battelle Press.
17. Harter, T., & Rollins, L. (2008). Watersheds, groundwater and drinking water: A practical guide. UCANR Publications.
18. Konečný, F., Boháček, Z., Müller, P., Kovářová, M., & Sedláčkov, I. (2002). Contamination of soils and groundwater by petroleum hydrocarbons and volatile organic compounds – Case study: ELSLAV BRNO. Bulletin of Geosciences, 78(3), 225–239.
19. Lake, L W.: Enhanced Oil Recovery. Prentice Hall Inc. (1989)
20. Martel, R., Gélinas, P. J., & Saumure, L. (1998). Aquifer washing by micellar solutions. *Journal of Contaminant Hydrology*, *30*(1–2), 33–48. https://doi.org/10.1016/S0169-7722(97)00031-4
21. Mayer, A. S. (2005). *Soil and groundwater contamination: Nonaqueous phase liquids*. American Geophysical Union.
22. Moran, W. M., & Losonsky, G. (Eds.). (2008). Enhanced delivery of potassium permanganate using horizontal wells (6th ed.). In *Proceedings of the Sixth International Conference on Remediation of Chlorinated and Recalcitrant Compounds*. Battelle Press.
23. Pennell, K. D., Jin, M., Abriola, L. M., & Pope, G. A. (1994). Surfactant enhanced remediation of soil columns contaminated by residual tetrachloroethylene. *Journal of Contaminant Hydrology*, *16*(1), 35–53. https://doi.org/10.1016/0169-7722(94)90071-X
24. Rao, D. N., Ayirala, S. C., Kulkarni, M. M., & Sharma, A. P. (2004, April). Development of gas assisted gravity drainage (GAGD) process for improved light oil recovery. In *SPE/DOE Symposium on Improved Oil Recovery*. Society of Petroleum Engineers. https://doi.org/10.2118/89357-MS
25. Roostapour, A., & Kam, S. I. (2012). Modeling foam delivery mechanisms in deep vadose zone remediation using method of characteristics. *Journal of Hazardous Materials*, *243*, 37–51. https://doi.org/10.1016/j.jhazmat.2012.09.014

26. Roostapour, A., Lee, G., Zhong, L., & Kam, S. I. (2014). Model fit to experimental data for foam-assisted deep vadose zone remediation. *Journal of Hazardous Materials*, *264*, 460–473. https://doi.org/10.1016/j.jhazmat.2013.09.016
27. Rosansky, S. (2020). *Application of horizontal wells to enhance site remediation* (TR-NAVFAC-EXWC-EV-2103). NAVFAC.
28. Rossen, W. R. (1996). Foams in enhanced oil recovery. In *Routledge eBooks* (pp. 413–464). https://doi.org/10.1201/9780203755709-11
29. Sawyer, C. S., & Lieuallen-Dulama, K. K. (1998). Productivity comparison of horizontal and vertical groundwater remediation well scenarios. *Ground Water*, *36*(1), 98–103. https://doi.org/10.1111/j.1745-6584.1998.tb01069.x
30. Sharma, P., Kostarelos, K., Lenschow, S., Christensen, A., & De Blanc, P. C. (2020). Surfactant flooding makes a comeback: Results of a full-scale, field implementation to recover mobilized NAPL. Journal of Contaminant Hydrology, 230, 103602. https://doi.org/10.1016/j.jconhyd.2020.103602
31. Stone, H. (1973). Probability model for estimating three-phase relative permeability. Journal of Petroleum Technology, 22(2), 214–218. https://doi.org/10.2118/2116-PA
32. Shiau, B., Hasagawa, M. A., Brammer, J. M., Carter, T., Goodspeed, M., Harwell, J. H., Sabatini, D. A., Knox, R. C., & Szekeres, E. (2002). Field demonstration of surfactant-enhanced DNAPL remediation: Two case studies. In ACS Symposium Series (Vol. 837, pp. 51–72). https://doi.org/10.1021/bk-2002-0837.ch004
33. Szafranski, R., Lawson, J. B., Hirasaki, J. G., Miller, C. A., Akiya, N., King, S., Jackson, R. E., Meinardus, H., & Londergan, J. (1998). Surfactant/foam process for improved efficiency of aquifer remediation. Progress in Colloid & Polymer Science, 111, 162–167.
34. United Nations. (2024). Water for prosperity and peace. UNESCO.